Purely numerical compensation for microscope objective phase curvature in digital holographic microscopy: influence of digital phase mask position

Frédéric Montfort, Florian Charrière, and Tristan Colomb

Ecole Polytechnique Fédérale de Lausanne (EPFL), Institut d'Optique Appliquée, CH-1015 Lausanne, Switzerland

Etienne Cuche

Lyncée Tec SA, PSE-A, CH-1005 Lausanne, Switzerland

Pierre Marquet

Centre de Neurosciences Psychiatriques, Département de Psychiatrie DP-CHUV, Site de Cery, 1008 Prilly-Lausanne, Switzerland

Christian Depeursinge

Ecole Polytechnique Fédérale de Lausanne (EPFL), Institut d'Optique Appliquée, CH-1015 Lausanne, Switzerland

Received March 17, 2006; revised June 1, 2006; accepted June 3, 2006; posted June 8, 2006 (Doc. ID 69123)

Introducing a microscope objective in an interferometric setup induces a phase curvature on the resulting wavefront. In digital holography, the compensation of this curvature is often done by introducing an identical curvature in the reference arm and the hologram is then processed using a plane wave in the reconstruction. This physical compensation can be avoided, and several numerical methods exist to retrieve phase contrast images in which the microscope curvature is compensated. Usually, a digital array of complex numbers is introduced in the reconstruction process to perform this curvature correction. Different corrections are discussed in terms of their influence on the reconstructed image size and location in space. The results are presented according to two different expressions of the Fresnel transform, the single Fourier transform and convolution approaches, used to propagate the reconstructed wavefront from the hologram plane to the final image plane.

OCIS codes: 090.1000, 090.1760, 100.3010, 110.0180.

1. INTRODUCTION

Because of the limited sampling capacity of the electronic camera compared with the one of photosensitive materials such as photographic plates, the spatial resolution of reconstructed images in digital holography was formerly limited compared with classical holography. Different approaches exist to achieve microscopic imaging with digital holography. One can, for example, use spherical diverging waves for the hologram recording, which allows a numerical enlargement of the object during the reconstruction process, without any image-forming lens, as described in Chap. 5 of Ref. 1. By the introduction of a microscope objective (MO), Cuche *et al.*[2] have demonstrated that digital holographic microscopy (DHM) allows one to reconstruct, with a lateral resolution below micrometers, the optical topography of specimens with a nanometric accuracy. Nevertheless, the introduction of a MO increases the complexity of the reconstruction process. Indeed, the MO introduces a phase curvature to the object wave that should be compensated perfectly to perform accurate measurement and imaging of the phase delay induced by the specimen. There are two different main possibilities to compensate for this phase curvature, either physically by introducing the same curvature in the reference wave or digitally as presented in Refs. 2–6.

The physical compensation, in standard interference microscopy like the Linnik configuration (see, for example, Chap. 20 in Ref. 7), is done experimentally by inserting the same MO in the reference arm, at equal distance from the exit of the interferometer. The curvature of the object wave is then compensated by the reference wavefront during interference. Nevertheless, this method requires a precise alignment of all the optical elements. Moreover, each modification in the object arm needs to be precisely reproduced in the reference arm.

In the present paper, we call digital phase mask (DPM) a complex numbers array, by which the reconstructed wavefront is multiplied during the hologram processing. Digitally, the definition and the position of the DPMs used to compensate the phase curvature can be different. Ferraro *et al.* make the compensation in the image plane by subtracting the reconstructed phase of a hologram ac-

quired without a specimen.[3] Cuche *et al.* define a numerical quadratic curvature model[2] that could be automatically computed in the image plane.[4] Finally, two recent papers show that the compensation for the MO curvature (and for phase aberrations) can be done in the hologram plane by using a reference hologram[5] or polynomial DPM models (standard or Zernike) computed automatically.[6] In spite of the numerous phase retrieval techniques proposed in the literature, no systematic study of the behavior of the phase images obtained through these reconstruction methods has, to our knowledge, been performed yet. In this paper, we present analytically the influence of the DPMs' position (hologram or image plane) in the reconstruction process, in particular in terms of position and size of the reconstructed specimen region of interest (ROI).

2. BASES OF DIGITAL HOLOGRAPHY

A. Principle and Reconstruction

Digital holography allows one to retrieve the original complex wavefront from an amplitude image, called a hologram, recorded on an electronic camera such as a CCD or complementary metal-oxide semiconductor camera. This hologram is created by the interference, in off-axis geometry, between two coherent waves: on one side the wave of interest, called object wave $\mathbf{O}$, coming from the object, and on the other a reference wave $\mathbf{R}$. In the hologram plane, the two-dimensional recorded intensity distribution $I_H(x,y)$ can be written[8] as

$$I_H(x,y) = |\mathbf{O}+\mathbf{R}|^2 = |\mathbf{O}|^2 + |\mathbf{R}|^2 + \mathbf{R}\mathbf{O}^* + \mathbf{R}^*\mathbf{O}, \tag{1}$$

where $\mathbf{R}^*\mathbf{O}$ and $\mathbf{R}\mathbf{O}^*$ are the interference terms with $\mathbf{R}^*$ and $\mathbf{O}^*$ denoting the complex conjugate of the two waves.

After hologram apodization[9] and spatial filtering,[10] the virtual interference term $\mathbf{R}^*\mathbf{O}$ (the same procedure can be done with the real interference term $\mathbf{R}\mathbf{O}^*$) is multiplied in the hologram plane by a DPM Γ^H,[5] which should be ideally equal to $\mathbf{R}$, to reproduce the original wavefront $\Psi^H = \mathbf{R}\mathbf{R}^*\mathbf{O} = \Gamma^H\mathbf{R}^*\mathbf{O}$ in the hologram plane. Once the wavefront Ψ^H has been retrieved, it has to be propagated to the image plane to have a focused image. This propagation of a monochromatic reconstructed wavefront Ψ^H at wavelength $\lambda = 2\pi/k$ from the hologram plane to the image plane over a distance d is done in the Fresnel approximation,[1–6,9–11] which allows one to implement numerically the propagation by simple fast Fourier transforms (FFTs), as will be pointed out further:

$$\Psi^I(x,y) = \frac{\exp(ikd)}{i\lambda d}\int\int \Psi^H(\xi,\eta) \times \exp\left\{ i\frac{\pi}{\lambda d}[(\xi-x)^2 + (\eta-y)^2]\right\} \mathrm{d}\xi\mathrm{d}\eta, \tag{2}$$

where Ψ^I is the corresponding wavefront propagated to the image plane. Let us define the two-dimensional Fresnel transform (FT) of parameter $\tau = \sqrt{\lambda d}$ of a given function $f(x,y)$ as

$$\mathcal{F}_\tau[f(x,y)] = \frac{1}{\tau^2}\int\int f(\xi,\eta) \times \exp\left\{ i\frac{\pi}{\lambda d}[(\xi-x)^2 + (\eta-y)^2]\right\} \mathrm{d}\xi\mathrm{d}\eta. \tag{3}$$

Using this definition, Eq. (2) can be written as

$$\Psi^I(x,y) = -i\exp(ikd)\mathcal{F}_{\sqrt{\lambda d}}[\Psi^H(x,y)]. \tag{4}$$

This analytical expression of propagation can be digitized by using two different formulations: the single FT and the convolution formulations.

1. Single Fourier-Transform Formulation

The propagation in the Fresnel approximation [Eq. (4)] can be written using a single FT:

$$\Psi^I(x,y) = \frac{\exp(ikd)}{i\lambda d}\exp\left[i\frac{\pi}{\lambda d}(x^2+y^2)\right] \times FT\left\{ \Psi^H(\xi,\eta)\exp\left[i\frac{\pi}{\lambda d}(\xi^2+\eta^2)\right]\right\}. \tag{5}$$

In its discrete formulation, the low time-consuming FFT algorithm can be employed.[2] In the following text, this formulation will be referred to as FT formulation.

In this case the sampling step of the propagated image is not the same as the initial one. If the initial image is given by $N_{\mathrm{pts}} \times N_{\mathrm{pts}}$ points with a sampling step $T_\xi \times T_\eta$, the image propagated over a distance d is sampled with the same number of points but with a sampling step given by

$$T_x = \frac{\lambda d}{N_{\mathrm{pts}} T_\xi}, \quad T_y = \frac{\lambda d}{N_{\mathrm{pts}} T_\eta}. \tag{6}$$

2. Convolution Formulation

The Fresnel propagation given by Eq. (4) can be written using a convolution formulation:

$$\Psi^I(x,y) = \frac{\exp(ikd)}{i\lambda d}[\Psi^H(x,y)] \otimes \exp\left[i\frac{\pi}{\lambda d}(x^2+y^2)\right]. \tag{7}$$

Its discrete form is a little more time-consuming than the FT formulation when computed.[1,12] The convolution expression of the propagation in the Fresnel approximation has the same sampling step before and after the propagation. Thus if the image in the hologram plane is sampled in $N_{\mathrm{pts}} \times N_{\mathrm{pts}}$ points with a sampling step $T_\xi \times T_\eta$, the propagated image is sampled with the same number of points and a sampling step $(T_x \times T_y) = (T_\xi \times T_\eta)$.

B. Microscope Objective Introduction

The introduction of a MO in the object arm opens the possibility of imaging at the submicrometer scale. As shown in Fig. 1, the optical arrangement in the object arm is that of an ordinary single-lens system producing a magnified image of the specimen in an image plane. In comparison with classical microscopy, the difference is that the CCD camera is not in the image plane but is in the hologram plane that is located between the MO and the image plane, at a distance d from the image. This situation can

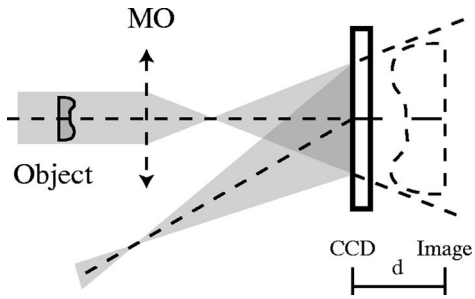

Fig. 1. Standard configuration in holographic microscopy: The CCD defining the hologram plane is placed in front of the image obtained though the microscope objective (MO). d is the reconstruction distance.

be considered to be equivalent to a holographic configuration without a MO with an object wave emerging directly from the image and not from the object itself.

The MO produces a curvature of the wavefront in the object arm. This deformation affects only the phase of the object wave and does not disturb amplitude contrast imaging. However, to perform an accurate measurement of the phase delay induced by the specimen only, the phase curvature induced by the MO must be perfectly compensated. This compensation can be done in the hologram plane by a DPM Γ^H and/or in the image plane by a DPM Γ^I. Therefore we can write the corrected wavefront generally as

$$\Upsilon^I(x,y) = -\Gamma^I i \exp(ikd)\mathcal{F}_{\sqrt{\lambda d}}[\Gamma^H \Psi^H(x,y)]. \tag{8}$$

3. HOLOGRAM RECONSTRUCTION: THE IDEAL CASE

Let us first express analytically the reconstruction process that exactly reproduces the image resulting from the object through the MO, as it would be performed on an optical bench, without any scaling or lateral or axial shifting. This ideal case formulation will serve as a gauge image for comparison with the images obtained by the different digital reconstruction methods.

The hologram is multiplied by an ideal DPM Γ^H_{id} corresponding to a replica of the reference wave:

$$\Psi^H_{\mathrm{id}} = \Gamma^H_{\mathrm{id}} \mathbf{R}^* \mathbf{O} = \mathbf{R}\mathbf{R}^* \mathbf{O} = \mathbf{O}, \tag{9}$$

where the reference wave amplitude has been assumed to be equal to one. The propagation over a distance d_{id} expressed using Eq. (4) is given by

$$\Psi^I_{\mathrm{id}} = -i \exp(ikd_{\mathrm{id}})\mathcal{F}_{\sqrt{\lambda d_{\mathrm{id}}}}[\Psi^H_{\mathrm{id}}], \tag{10}$$

$$= -i \exp(ikd_{\mathrm{id}})\mathcal{F}_{\sqrt{\lambda d_{\mathrm{id}}}}[\mathbf{O}], \tag{11}$$

where Ψ^I_{id} corresponds to the exact initial object wavefront.

In a general approach, we can consider an off-axis microscopy setup (angle θ between the propagation direction of the reference and object waves), in which the curvatures of the reference and object waves at the hologram plane are different (Fig. 2). Let us define the centers of the spherical reference and object waves as

$$S_R = [S_{Rx}, S_{Ry}, (h_r^2 - S_{Rx}^2 - S_{Ry}^2)^{1/2}], \tag{12}$$

$$S_O = [0, 0, h_o], \tag{13}$$

where h_r and h_o are, respectively, the distances between the source points of the reference and object waves and the recombining location of the two beams. Note that the source point of the spherical object wave is located at the back focal plane of the MO. The reference wavefront in the hologram plane is thus given by[8]

$$\mathbf{R}(x,y) = \exp\left\{ i \frac{\pi}{\lambda h_r}[(x - S_{Rx})^2 + (y - S_{Ry})^2] \right\}. \tag{14}$$

Let us now define a blank object wave $\mathbf{O}_0$ (without a specimen in the transmission configuration and with a flat surface in the reflection configuration).[4] Because we assumed that only phase curvature is induced by the MO, the wavefront of the blank object wave at the hologram plane is

$$\mathbf{O}_0(x,y) = \exp\left[i \frac{\pi}{\lambda h_o}(x^2 + y^2) \right]. \tag{15}$$

To recover the phase delay induced by the object only, the phase curvature induced by both the MO and the reference beam curvatures can be compensated by multiplying Ψ^I_{id} by a second DPM Γ^I_{id} introduced in the image plane. The latter is determined by the complex conjugate of the blank wave $\mathbf{O}_0$ propagated to the image plane:

$$\Gamma^I_{\mathrm{id}} = \{\mathcal{F}_{\sqrt{\lambda d_{\mathrm{id}}}}[\Psi^H_{\mathrm{id},0}]\}^*, \tag{16}$$

$$= \{\mathcal{F}_{\sqrt{\lambda d_{\mathrm{id}}}}[\mathbf{O}_0]\}^*. \tag{17}$$

The corrected wavefront Υ^I_{id} becomes

$$\Upsilon^I_{\mathrm{id}} = \Gamma^I_{\mathrm{id}} \Psi^I_{\mathrm{id}}, \tag{18}$$

$$= \{\mathcal{F}_{\sqrt{\lambda d_{\mathrm{id}}}}[\mathbf{O}_0]\}^* \mathcal{F}_{\sqrt{\lambda d_{\mathrm{id}}}}[\mathbf{O}]. \tag{19}$$

Inserting Eqs. (14) and (15), Eqs. (17) and (18) can be written as

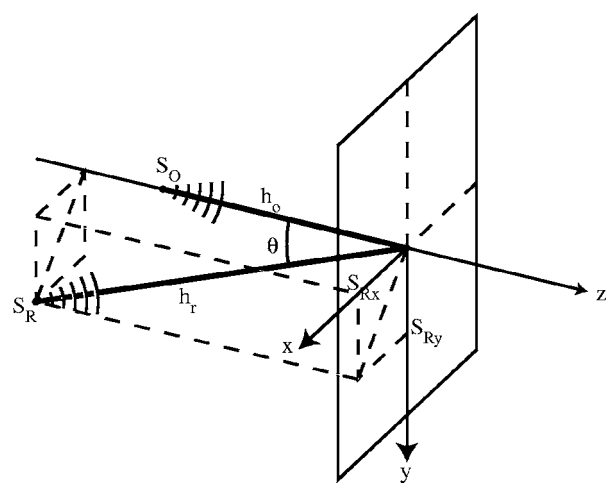

Fig. 2. Schema of the used notations.

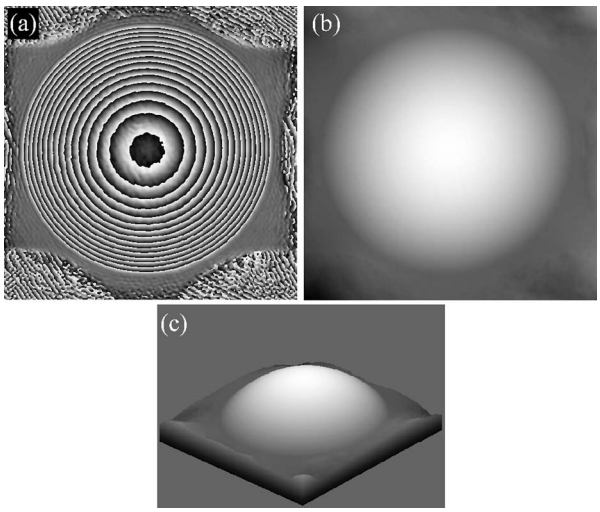

Fig. 3. (a) Phase reconstruction of the microlens recorded in a transmission DHM setup (diameter 240 μm, height 21.15 μm), (b) two-dimensional unwrap of (a), (c) perspective representation of (b).

$$\Gamma_{\mathrm{id}}^{I}(x,y) = \exp\left[-i\frac{\pi}{\lambda(h_o + d_{\mathrm{id}})}(x^2+y^2)\right], \tag{20}$$

$$\Upsilon_{\mathrm{id}}^{I}(x,y) = -i\exp(ikd_{\mathrm{id}}) \times \exp\left[-i\frac{\pi}{\lambda(h_o + d_{\mathrm{id}})}(x^2+y^2)\right]\mathcal{F}_{\sqrt{\lambda d_{\mathrm{id}}}}[\Psi_{\mathrm{id}}^{H}]. \tag{21}$$

Γ_{id}^{I} logically corresponds to the spherical wavefront centered in S_O at a distance $h_o + d_{\mathrm{id}}$ from the image plane.

This general development expresses the retrieval of the object wavefront, in which the MO curvature is corrected. Potentially this approach may also be used for correction of optical aberrations of the holographic setup,[4] but the development will be restricted to the case without aberrations, focusing on the effect of the phase curvature compensation.

4. PHASE CURVATURE COMPENSATION DURING NUMERICAL RECONSTRUCTION

To illustrate the different reconstruction approaches and propagation formulations, a hologram of a quartz microlens recorded in a transmission DHM setup with a 20× MO (numerical aperature of 0.5) is used. This microlens has a diameter of 240 μm and a height of 21.15 μm. Figures 3(a)–3(c) present the raw phase reconstruction, the two-dimensional unwrapped phase image, and its three-dimensional representation, respectively. The different notations for the approaches are done with a subscript letter: no letter, general; i, image plane; h, hologram plane; and m, mixed.

A. General Approach

Let us develop the general approach in which a DPM is introduced both in the hologram plane and in the image plane. The application of this general approach is developed in detail and illustrated with examples in Ref. 6. We first apply a DPM Γ^H to the interference term $\mathbf{R}^*\mathbf{O}$ in the hologram plane,

$$\Psi^H = \Gamma^H \mathbf{R}^*\mathbf{O}. \tag{22}$$

Propagating the resulting wave over a distance d to the image plane yields Ψ^I;

$$\Psi^I = -i\exp(ikd)\mathcal{F}_{\sqrt{\lambda d}}[\Psi^H], \tag{23}$$

$$= -i\exp(ikd)\mathcal{F}_{\sqrt{\lambda d}}[\Gamma^H\mathbf{R}^*\mathbf{O}]. \tag{24}$$

Then a second DPM Γ^I is applied in the image plane to compensate for the curvature of the propagated wavefront. The corrected wavefront Υ^I is thus given by

$$\Upsilon^I = \Gamma^I\Psi^I, \tag{25}$$

$$= -i\exp(ikd)\Gamma^I\mathcal{F}_{\sqrt{\lambda d}}[\Gamma^H\mathbf{R}^*\mathbf{O}]. \tag{26}$$

To determine the effects of Γ^H on the propagation, we will compare Υ^I with Υ_{id}^I obtained in the ideal case [see Eqs. (19) and (21)].

The DPM applied in the image plane for the phase curvature compensation will of course depend on the DPM introduced in the hologram plane. We defined the digital reference wave using the same notation as in the ideal case in Eqs. (14) and (12). In this way we can define a general DPM in the hologram plane. As it is supposed to be a curvature correction term, it is defined as the conjugate of a spherical wave centered in S_D:

$$\Gamma^H = \exp\left\{-i\frac{\pi}{\lambda h_d}[(x-S_{Dx})^2 + (y-S_{Dy})^2]\right\}, \tag{27}$$

$$S_D = [S_{Dx}, S_{Dy}, (h_d^2 - S_{Dx}^2 - S_{Dy}^2)^{1/2}]. \tag{28}$$

The DPM Γ^I in the image plane that compensates the resulting propagated wavefront is then given by

$$\begin{aligned}\Gamma^I(x,y) = {} & \exp\left(-i\frac{\pi[(S_{Dx}-S_{Rx})^2 + (S_{Dy}-S_{Ry})^2]}{\lambda(h_d - h_r)}\right) \\ & \times \exp\left(i\frac{\pi}{\lambda(h + d/M)}\left\{\frac{1}{M^2}\left[x - h\left(\frac{S_{Rx}}{h_r} - \frac{S_{Dx}}{h_d}\right)\right]^2 + \frac{1}{M^2}\left[y - h\left(\frac{S_{Ry}}{h_r} - \frac{S_{Dy}}{h_d}\right)\right]^2\right\}\right) \\ & \times \exp\left(-i\frac{\pi}{\lambda(h_0 + d/M)}\left\{\frac{1}{M^2}\left[x - d\left(\frac{S_{Rx}}{h_r} - \frac{S_{Dx}}{h_d}\right)\right]^2 + \frac{1}{M^2}\left[y - d\left(\frac{S_{Ry}}{h_r} - \frac{S_{Dy}}{h_d}\right)\right]^2\right\}\right),\end{aligned} \tag{29}$$

where M and h are defined as

$$h = \frac{h_d h_r}{h_d - h_r}, \quad M = \frac{h-d}{h}. \tag{30}$$

Finally, the phase curvature-corrected wavefront in the image plane Υ^I is given by

$$\begin{aligned}\Upsilon^I(x,y) &= \Gamma^I(x,y)\Psi^I(x,y)\\ &= -i\exp(ikd)\frac{1}{M}\mathcal{F}_{\sqrt{\lambda d/M}}(x',y')\\ &\quad\times\exp\left(-i\frac{\pi}{\lambda(h+d/M)}\left\{\frac{1}{M^2}\left[x-h\left(\frac{S_{Rx}}{h_r}-\frac{S_{Dx}}{h_d}\right)\right]^2\right.\right.\\ &\quad\left.\left.+\frac{1}{M^2}\left[y-h\left(\frac{S_{Ry}}{h_r}-\frac{S_{Dy}}{h_d}\right)\right]^2\right\}\right)\\ &= \exp\left[ik\left(d-\frac{d}{M}\right)\right]\frac{1}{M}\Upsilon^H_{\mathrm{id}}(x',y'),\end{aligned} \tag{31}$$

where $x'=[x-d(S_{Rx}/h_r-S_{Dx}/h_d)]M$ and $y'=[y-d(S_{R4}/h_r-S_{D4}/h_d)]M$. The propagation direction is no longer parallel to the optical axis, but is given by the angle θ:

$$\sin\theta=\frac{S_{Rx}^2+S_{Ry}^2}{h_r}-\frac{S_{Dx}^2+S_{Dy}^2}{h_d}. \tag{32}$$

By analyzing the image plane DPM given by Eq. (29), we can find that the first term is a phase constant of no particular interest and can be suppressed. The second term is compensating for the phase deformation induced by the reference wave and the DPM in the hologram plane. Finally the third term is the correction term of the object wavefront curvature. The final image Υ^I is a replica of the ideal case image scaled by a factor M and laterally shifted.

We note that one can retrieve the results of the ideal approach by setting $\Gamma^H=\mathbf{R}$:

$$\Gamma^H=\mathbf{R}\Rightarrow S_D=S_R,\quad h_d=h_r\Rightarrow\lim_{h_d\to\infty}h=h_r,\quad M=1,$$

which gives the well-known results of Eqs. (10), (20), and (21):

$$\lim_{\Gamma^H\to R}\Psi^I(x,y)=\Psi^I_{\mathrm{id}}(x,y), \tag{33}$$

$$\lim_{\Gamma^H\to R}\Gamma^I(x,y)=\exp\left[-i\frac{\pi(x^2+y^2)}{\lambda(h_o+d)}\right], \tag{34}$$

$$\lim_{\Gamma^H\to R}\Upsilon^I(x,y)=-i\exp(ikd)\times\exp\left[-i\frac{\pi(x^2+y^2)}{\lambda(h_o+d)}\right]\Psi^I_{\mathrm{id}}(x,y). \tag{35}$$

B. Image Plane Approach

In the case of the image plane approach, no DPM is applied in the hologram plane and the propagating term is $\mathbf{R}^*\mathbf{O}$, the illumination wave being considered of unit intensity. This can be seen as if the hologram would be reconstructed with a plane wave propagating along the optical axis (Fig. 4).

The phase curvature compensation process is therefore applied to the propagated interference term $\mathbf{R}^*\mathbf{O}$. The DPM can be computed from known flat areas on the specimen with the procedure described in Ref. 4 or from the propagation of a blank hologram as described in Ref. 3. This DPM is given by

$$\Gamma_i^I=\{\mathcal{F}_{\sqrt{\lambda d_i}}[\mathbf{R}^*\mathbf{O}_0]\}^*. \tag{36}$$

The flattened wavefront Υ_i^I can be written as

$$\Upsilon_i^I=-i\exp(ikd_i)\{\mathcal{F}_{\sqrt{\lambda d_i}}[\mathbf{R}^*\mathbf{O}_0]\}^*\mathcal{F}_{\sqrt{\lambda d_i}}[\mathbf{R}^*\mathbf{O}]. \tag{37}$$

The condition $\Gamma^H=1$ imposes the following:

$$S_D=0,\quad\lim_{\Gamma^H\to 1}h_d=\infty,\quad\frac{S_D}{h_d}=0,$$

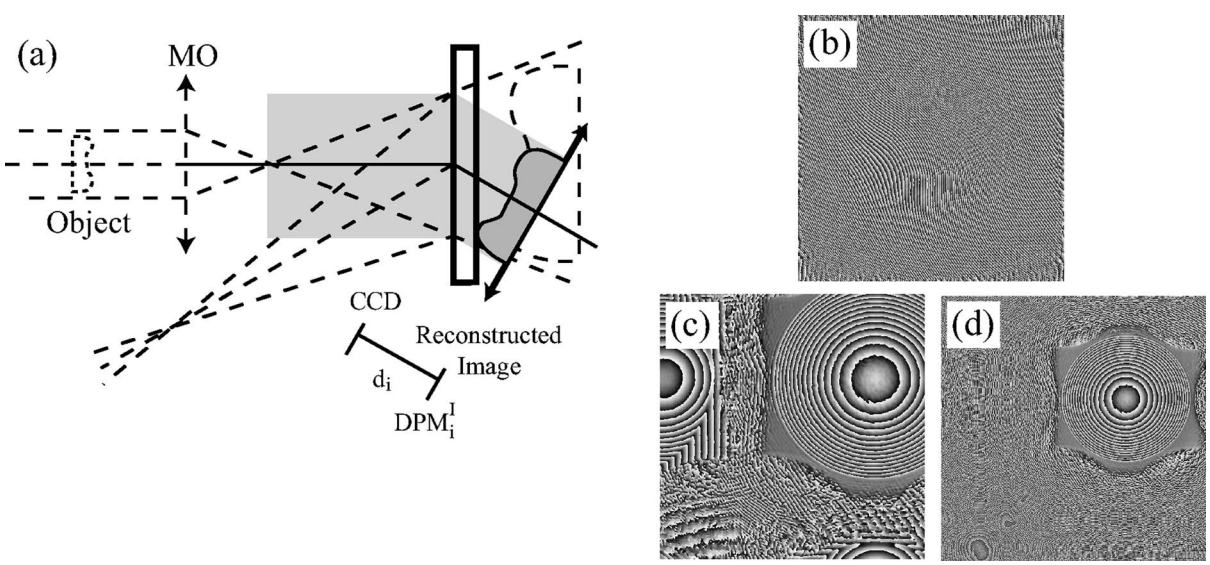

Fig. 4. (a) Reconstruction in the image plane approach: The illumination beam is a plane wave propagating along the optical axis. The phase curvature is compensated in the image plane. The reconstructed image is not the image of the object through the MO (shown by a dashed line). (b) Phase image in the hologram plane. (c) and (d) Phase images in the image plane in convolution and FT formulations, respectively.

$$\Rightarrow \lim_{h_d\to\infty} h = h_r, \quad \lim_{h_d\to\infty} M = \frac{h_r - d}{h_r} = M_i.$$

Introducing these results in Eqs. (29) and (31), we can express the DPM Γ_i^I that expresses the phase curvature correction leading to the expression of the corrected image wavefront Υ_i^I:

$$\Gamma_i^I(x,y) = \lim_{\Gamma^H\to 1} \Gamma^I(x,y) = \exp\left\{ i\frac{\pi}{\lambda(h_r + d_i/M_i)}\left[\frac{1}{M_i^2}(x - S_{Rx})^2 + \frac{1}{M_i^2}(y - S_{Ry})^2\right]\right\}\exp\left\{-i\frac{\pi}{\lambda(h_0 + d_i/M_i)}\left[\frac{1}{M_i^2}\times\left(x - \frac{d_i}{h_r}S_{Rx}\right)^2 + \frac{1}{M_i^2}\left(y - \frac{d_i}{h_r}S_{Ry}\right)^2\right]\right\}, \tag{38}$$

$$\Upsilon_i^I(x,y) = \lim_{\Gamma^H\to 1} \Upsilon^I(x,y) = -i\exp\left[ik\left(d_i - \frac{d_i}{M}\right)\right] \times \frac{1}{M_i}\Upsilon_{\mathrm{id}}^I\left(\frac{x - \frac{d_i}{h_r}S_{Rx}}{M_i}, \frac{y - \frac{d_i}{h_r}S_{Rx}}{M_i}\right). \tag{39}$$

Equation (39) shows that the correction in the image plane approach also introduces a resizing of the image in comparison with the ideal case. The scale factor is a function of the reference beam curvature h_r. This scaling is due to the fact that, compared with the ideal solution, the correction of the reference curvature is not performed in the hologram plane as it is when the hologram is processed with exactly the same reference wave used during acquisition.

In the image plane approach, the image is also laterally shifted in space, as mentioned in the general approach and shown in Fig. 4. The shift is due to the fact that the propagation direction is modified by an angle θ from the optical axis of the object beam. θ is given by

$$\sin\theta = \frac{S_{Rx}^2 + S_{Ry}^2}{h_r}. \tag{40}$$

This inclination of the propagation direction arises from the fact that the illumination wave propagates along the optical axis, which is precisely inclined of an angle θ from the correct reference wave. This induced error corresponds to a tilt of the wavefront that is not corrected in the hologram plane and induced this propagation deviation. The lateral shift is thus given by

$$L_{\mathrm{shift}} = \frac{d_i}{h_r}(S_{Rx}^2 + S_{Ry}^2)^{1/2} = d_i \sin\theta. \tag{41}$$

This shift is not convenient for the numerical propagation. Indeed, the image is no longer centered in the reconstruction window. In a convolution formulation of the propagation (see subsection 5.B), this results in a tailed image [Fig. 4(c)]. In the case of the FT formulation, it may not be a problem if the sampling step is small enough so that the field of view of the window is large enough to cover the off-axis propagating wavefront [Fig. 4(d)]. The mixed approach will give a solution in which the reconstructed image has the same size and sampling step as the reconstructed image in the image plane approach, but without lateral shift (Fig. 5).

C. Hologram Plane Approach

In this second digital approach, a single DPM is applied in the hologram plane.[5] Thus the considered wavefront is directly $\mathbf{R}^*\mathbf{O}$. Let us suppose a recording of a reference hologram, where no object is present in the object beam. The recorded term is then given by $\mathbf{R}^*\mathbf{O}_0$. Its conjugate defines perfectly the DPM to be applied in the hologram plane:

$$\Gamma_h^H = \mathbf{R}\mathbf{O}_0^*. \tag{42}$$

By multiplying the interference term by the DPM and expressing the result as a function of the ideal retrieved wavefront, we obtain [Fig. 6(b)]:

$$\Psi_h^H = \Gamma_h^H\mathbf{R}^*\mathbf{O} = \mathbf{O}_0^*\Psi_{\mathrm{id}}^H = \Upsilon_h^H. \tag{43}$$

Thus the propagation of this resulting wavefront over a distance d_h to the image plane can be expressed as

$$\Upsilon_h^I = -i\exp(ikd_h)\mathcal{F}_{\sqrt{\lambda d_h}}[\Psi_h^H] = -i\exp(ikd_h)\mathcal{F}_{\sqrt{\lambda d_h}}[\mathbf{O}_0^*\mathbf{O}]. \tag{44}$$

The interference term has been at the same time multiplied by the illumination wave $\mathbf{R}$ and by the correction term that compensates for the object wavefront curvature. The result is a plane wave modulated by the object-related phase variations. Its propagation will therefore be a plane wave and no curvature compensation will be needed at any reconstruction distance, in particular in the focused image plane (Fig. 6).

Nevertheless, the multiplication, in the hologram plane already, of the interference term by the curvature compensation term has an influence on the image. Indeed, the propagated wavefront is $\mathbf{O}_0^*\mathbf{O}$ instead of $\mathbf{O}$ in the ideal case, which influences the focus distance, image size, etc.

In the case of a microscope without aberrations, the term $\mathbf{O}_0^*$ compensating the curvature of the MO corresponds to the transfer function of a lens. The corrected wavefront in the image plane Υ_h^I is given by

$$\Upsilon_h^I(x,y) = -i\exp(ikd_h) \times \mathcal{F}_{\sqrt{\lambda d_h}}\left\{\exp\left[-i\frac{\pi}{\lambda h_o}(x^2 + y^2)\right]\Psi_{\mathrm{id}}^H(x,y)\right\} \tag{45}$$

$$= \exp\left[ik\left(d_h - \frac{d_h}{M_h}\right)\right]\frac{1}{M_h}\Upsilon_{\mathrm{id}}^I\left(\frac{x}{M_h}, \frac{y}{M_h}\right). \tag{46}$$

The algorithm compensating for the phase curvature is thus equivalent to the insertion of a numerical lens in the hologram plane. We note that the focal length is determined only by the object wave shape and is totally independent of the reference wavefront, which has been compensated by the DPM.

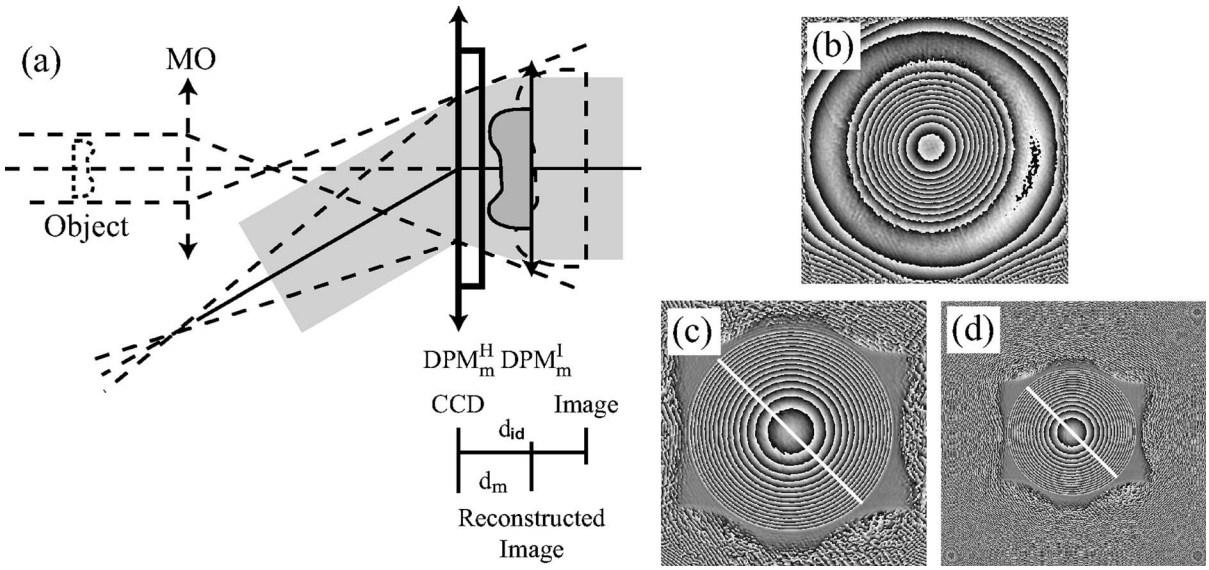

Fig. 5. (a) Reconstruction in the mixed approach: The illumination beam is a plane wave propagating along the reference wave axis. The first-order DPM is applied in the hologram plane and a second of higher orders in the image plane. The reconstructed image is not the image of the object through the MO (shown by a dashed line). (b) Phase image in the hologram plane. (c) and (d) Phase images in the image plane in convolution and FT formulations, respectively. The white lines define the diameter of the microlens diameter to be compared with Fig. 6

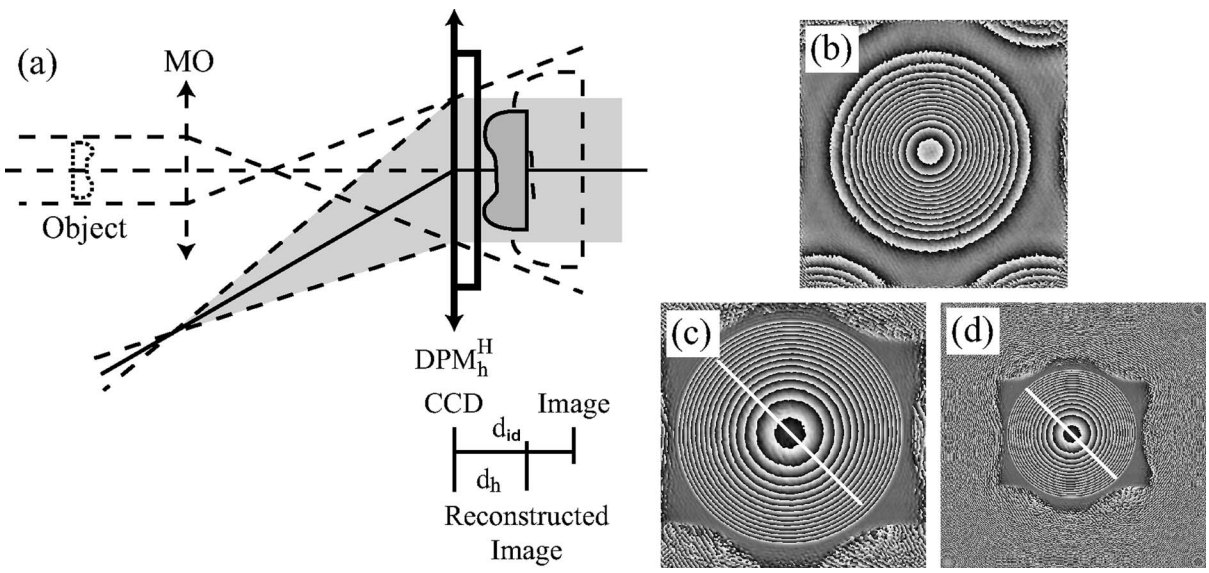

Fig. 6. (a) Reconstruction in the hologram plane approach: The illumination beam is a replica of the reference beam. The phase curvature is compensated in the hologram plane. The reconstructed image is not the image of the object through the MO (shown by a dashed line). (b) Phase image in the hologram plane. (c) and (d) Phase images in the image plane in convolution and FT formulations, respectively. The white lines define the diameter of the microlens reconstructed with the mixed approach (Fig. 5).

The resulting image Υ_h^H is thus focused at a distance d_h and magnified by a factor M_h given by the thin-lens relation:

$$\frac{1}{h_o} = -\frac{1}{d_{\mathrm{id}}} + \frac{1}{d_h}, \quad M_h = \frac{d_h}{d_{\mathrm{id}}}, \tag{47}$$

where h_o is the focal length of the introduced numerical lens, and d_{id} is the focus distance of the reconstructed image in the ideal case (equal to the distance between the image of the object through the MO and the hologram plane). We note that h_o corresponds to the distance between the back focal plane of the MO and the hologram plane.

D. Mixed Approach

The mixed approach is a method combining both the hologram and the image plane approaches. It consists in defining the DPM in the hologram plane keeping account of only some selected polynomial orders for a partial hologram plane correction. After propagation, an image plane DPM is defined and the remaining polynomial orders are corrected. Several combinations are possible depending on which orders are corrected in the hologram plane. Nev-

ertheless, only the case of the first-order phase correction, i.e., planar phase correction, in the hologram plane will be discussed. This corresponds to illuminating the hologram with a plane wave having the same propagation direction as the reference wave. It is thus similar to the image plane approach, except that the illumination wave has the same propagation direction as the reference wave instead of the object wave (Fig. 5).

In the hologram plane, the interference term $\mathbf{R}^*\mathbf{O}$ is multiplied by a first-order DPM corresponding to a plane wave (PW_m^H) [Fig. 5(b)]:

$$\Gamma_m^H = PW_m^H = \exp\left[-i\frac{2\pi}{\lambda}\left(\frac{S_{Rx}}{h_r}x + \frac{S_{Ry}}{h_r}y\right)\right]. \tag{48}$$

The determination of Γ_m^I results in

$$\Gamma_m^I(x,y) = \left\{PW_m^H(x,y) \times \mathcal{F}_{\sqrt{\lambda d_m}}\left[\mathbf{R}^*\mathbf{O}\left(x + \frac{d_m}{h_r}S_{Rx}, y + \frac{d_m}{h_r}S_{Ry}\right)\right]\right\}^*, \tag{49}$$

and the corrected wavefront Υ_m^I in the image plane is given by

$$\Upsilon_m^I(x,y) = -i\exp(ikd_m)\Gamma_i^I\left(x + \frac{d_m}{h_r}S_{Rx}, y + \frac{d_m}{h_r}S_{Ry}\right) \times \mathcal{F}_{\sqrt{\lambda d_m}}\left[\mathbf{R}^*\mathbf{O}\left(x + \frac{d_m}{h_r}S_{Rx}, y + \frac{d_m}{h_r}S_{Ry}\right)\right]. \tag{50}$$

The comparison of Υ_m^I with Υ_i^I given by Eq. (37) indicates that the reconstructed images are exactly the same in both cases, but spatially located at different positions. Indeed, the propagation in the mixed approach deviates by an angle $-\theta$ from the image plane approach, where θ is given by Eq. (40), which means that the reconstructed wavefront is again propagating along the optical axis. In the case without aberrations, the mixed approach is a particular case of the general approach in which $\Gamma^H = PW_m^H$:

$$\Gamma^H = PW_m^H \Rightarrow S_D \to \infty, \quad h_d \to \infty, \quad \frac{S_D}{h_d} = \frac{S_R}{h_r},$$

$$\Rightarrow \lim_{h_d\to\infty} h = h_r, \quad \lim_{h_d\to\infty} M = \frac{h_r - d}{h_r} = M_i.$$

Using Eqs. (29) and (31), we can express the DPM Γ_m^I for phase correction:

$$\Gamma_m^I(x,y) = \Gamma^I(x,y)|_{\Gamma^H = PW_m^H} = \exp\left[i\frac{\pi}{\lambda(h_r + d_m/M_i)}\left(\frac{x^2}{M_i^2} + \frac{y^2}{M_i^2}\right)\right] \times \exp\left[-i\frac{\pi}{\lambda(h_0 + d_m/M_i)}\left(\frac{x^2}{M_i^2} + \frac{y^2}{M_i^2}\right)\right], \tag{51}$$

which leads to the expression of the curvature-compensated image wavefront Υ_m^I:

$$\Upsilon_m^I(x,y) = \Upsilon^I(x,y)|_{\Gamma^H = PW_m^H} \tag{52}$$

$$= \exp\left[ik\left(d_m - \frac{d_m}{M_i}\right)\right]\frac{1}{M_i}\Upsilon_{\mathrm{id}}^I\left(\frac{x}{M_i}, \frac{y}{M_i}\right). \tag{53}$$

These results show that the reconstructed image is the same as the one issued from the image plane approach, except that it is centered on the optical axis. The scaling factor and propagation distance are the same. The effect of the first-order correction in the hologram plane is to center the image on the optical axis. This mixed approach is thus interesting in the sense that it can be applied to the convolution approach of the Fresnel propagation.

5. DISCUSSION

A. Analytical Formulation

It has been shown that in the image plane approach, the reference wave may induce some differences compared with the ideal case, as the phase curvature correction is not performed in the hologram plane, but only in the image plane. In the hologram plane approach, the difference with the ideal case is due to the correction of the object wave curvature, already performed in the hologram plane, the consequences therefore depending on the shape of the object wavefront. Finally, the mixed approach reduces the difference between the image approach and the ideal case by correcting the propagation direction. Table 1 summarizes quantitatively the consequences in terms of magnification and shift for each approach.

Each of these approaches has its own particularities. The hologram plane approach has the advantage of propagating, along the optical axis, a wave containing only the phase deformations due to the object. The phase modulations induced by the object are most often weak and the wave propagates quite like a plane wave, meaning that the phase curvature is compensated for any propagation distance. As the DPM is applied in the fixed hologram plane, it does not depend on the reconstruction distance like in the image plane approach. Thus the DPM can be determined once for a given setup, which is of great interest in automated reconstruction processes. The drawback of this solution is that the image is not focused in the hologram plane. Thus, the areas used for the fit of the DPM[6] are disturbed by the diffraction pattern of the object. The DPM determined in the hologram approach may thus be approximative in some cases, and may need a minor adjustment in the image plane, creating a particular mixed approach.

The image plane approach has the opposite arguments. It has the advantage of a focused image, and therefore clear constant phase areas are available around the object to perform the phase compensation procedure. This advantage is balanced with the fact that the phase curvature is not compensated for any reconstruction distance

and that the image is not centered in the reconstruction window. Only the presented mixed approach corrects this last disadvantage.

B. Discrete Formulation

All the considerations on the reconstruction approach are done considering continuous functions. Nevertheless, the sampling of the image and the propagation method have an influence on the size of the reconstructed images.

The continuous expression of the resulting image Υ^I in the different propagation methods can be summarized by the expression

$$\Upsilon^I(x,y) = \exp\left[ik\left(d - \frac{d}{M}\right)\right]\frac{1}{M}\Upsilon_{\mathrm{id}}^H\left(\frac{x-a}{M},\frac{y-b}{M}\right). \quad (54)$$

The ideal case corresponds to $d = d_{\mathrm{id}}$, $M = 1$, $a = b = 0$. As defined in the different reconstruction approaches, the focusing distance d and the magnification ratio M are given by

$$M = \frac{d}{d_{\mathrm{id}}}. \quad (55)$$

Considering these expressions, let us define the image sizes in the discrete formulation using both the convolution and FFT expression of the propagation.

1. Fourier Transform Formulation

Using the FT formulation of the propagation [Eq. (5)], Υ^I is expressed as

$$\Upsilon^I(n,m) = \exp\left[ik\left(d - \frac{d}{M}\right)\right]\frac{1}{M} \times \Upsilon_{\mathrm{id}}^H\left((n-a_\xi)\frac{\lambda d}{N_{\mathrm{pts}}T_\xi}\frac{1}{M},\ (m-b_\eta)\frac{\lambda d}{N_{\mathrm{pts}}T_\eta}\frac{1}{M}\right). \quad (56)$$

In the digital reconstruction, the focusing distance is given from Eq. (56):

$$d = Md_{\mathrm{id}}. \quad (57)$$

Inserting Eq. (58) into Eq. (57), we obtain

$$\Upsilon^I(n,m) = \exp\left[ik\left(d - \frac{d}{M}\right)\right]\frac{1}{M} \times \Upsilon_{\mathrm{id}}^H\left((n-a_\xi)\frac{\lambda d_{\mathrm{id}}}{N_{\mathrm{pts}}T_\xi},\ (m-b_\eta)\frac{\lambda d_{\mathrm{id}}}{N_{\mathrm{pts}}T_\eta}\right) = \Upsilon_{\mathrm{id}}^I(n-a_\xi, m-b_\eta). \quad (58)$$

This last result shows that the multiplication of the wavefront by a quadratic DPM in the hologram plane has no influence on the resulting image size. The FT formulation of the propagation is thus not sensitive to scaling induced by the different reconstruction methods [see Figs. 4(d), 5(d), and 6(d)].

As presented extensively in Ref. 1, one seems at first sight to lose (or gain) resolution by applying the FFT version. On closer examination one recognizes that $\lambda d/N_{\mathrm{pts}}T_\xi$ corresponds to the resolution limit given by the diffraction theory of optical systems: The hologram is the aperture of the optical system with side length $N_{\mathrm{pts}} \times T_\xi$. According to the theory of diffraction, at a distance d behind the hologram a diffraction pattern develops. $T_x = \lambda d/N_{\mathrm{pts}}T_\xi$ is therefore the diameter of the Airy disk (or speckle diameter) in the plane of the reconstructed image, which limits the resolution. This can be regarded as the automatic scaling algorithm, setting the resolution of the image reconstructed in the Fresnel approximation by a FFT always to the physical limit. The numerical lens inserted by the reconstruction algorithm thus has no effect.

2. Convolution Formulation

It has already been shown that the convolution expression [Eq. (7)] of the propagation in the Fresnel approximation has the same sampling step before and after the propagation. This means that the image is sampled in the same manner in the hologram plane than in the image plane. Υ^I can be written as

Table 1. Summary of the Different Reconstructed Image Properties

Approach	Υ	Magnification	Shift
Ideal	$\Upsilon_{\mathrm{id}}(x,y)$	1	(0, 0)
Hologram plane	$\exp[ik(d-d_{\mathrm{id}})]\frac{1}{M_h}\Upsilon_{\mathrm{id}}^I\left(\frac{x}{M_h},\frac{y}{M_h}\right)$	$\frac{h_o-d}{h_o}$	(0, 0)
Image plane	$\exp[ik(d-d_{\mathrm{id}})]\frac{1}{M_h}\Upsilon_{\mathrm{id}}^I\left(\frac{x-\frac{d}{h_r}S_{Rx}}{M_i},\frac{y-\frac{d}{h_r}S_{Ry}}{M_i}\right)$	$\frac{h_r-d}{h_r}$	$\left(\frac{d}{h_r}S_{Rx},\frac{d}{h_r}S_{Ry}\right)$
Mixed	$\exp[ik(d-d_{\mathrm{id}})]\frac{1}{M_i}\Upsilon_{\mathrm{id}}^I\left(\frac{x}{M_i},\frac{y}{M_i}\right)$	$\frac{h_r-d}{h_r}$	(0, 0)

$$\Upsilon^I(n,m) = \exp\left[ik\left(d - \frac{d}{M}\right)\right]\frac{1}{M}\Upsilon^H_{\mathrm{id}}\left(\frac{(n-a_\xi)T_\xi}{M}, \frac{(m-b_\eta)T_\eta}{M}\right), \tag{59}$$

which means that the size of the images is magnified the same way as in the continuous domain. Figure 6(c) is reconstructed using the hologram plane approach. The image has the same size as the hologram. Figure 5(c) is reconstructed using the mixed approach. The size of the images of Figs. 5(c) and 5(d) is not the same because the magnification factor with respect to the ideal case is different. Reconstruction of holograms by the convolution approach results indeed in images with more or fewer pixels per unit length than those reconstructed by the FFT. However, because of the physical limits, the image resolution does not change.

6. CONCLUSION

In digital holography, the access to numerical data allows an easy compensation of the nondesired phase curvatures in the reconstructed images. Nevertheless, procedures are required to determine the correction to be applied. The recorded data, corresponding to the interference term $\mathbf{R}^*\mathbf{O}$, usually do not allow the retrieval of the original image, but only a scaled replica displaced both laterally and axially. The reconstructed image can therefore be considered to be an image of the object through a system, composed of a MO and an additional numerical lens, that can be analytically characterized to get the exact properties of the complete holographic microscope. In this paper, we have presented for the first time to our knowledge the influence of the phase masks' position involved in the reconstruction process, in particular in terms of position and size of the reconstructed specimen ROI.

We hope that this study on the reconstruction methods, in conjunction with the remarks on the reconstructed image sampling regarding the FT or convolution formulation, will clarify the relations subtended between the available hologram processing techniques, facilitating the user's choice for each specific application of DHM.

ACKNOWLEDGMENT

This work was funded through research grants 205320-103885/1 from the Swiss National Science Foundation.

The e-mail address for F. Montfort is frederic.montfort@a3.epfl.ch.

REFERENCES

1. U. Schnars and W. P. O. Jüptner, "Digital recording and numerical reconstruction of holograms," Meas. Sci. Technol. **13**, R85–R101 (2002).
2. E. Cuche, P. Marquet, and C. Depeursinge, "Simultaneous amplitude-contrast and quantitative phase-contrast microscopy by numerical reconstruction of Fresnel off-axis holograms," Appl. Opt. **38**, 6994–7001 (1999).
3. P. Ferraro, S. D. Nicola, A. Finizio, G. Coppola, S. Grilli, C. Magro, and G. Pierattini, "Compensation of the inherent wave front curvature in digital holographic coherent microscopy for quantitative phase-contrast imaging," Appl. Opt. **42**, 1938–1946 (2003).
4. T. Colomb, E. Cuche, F. Charrière, J. Kühn, N. Aspert, F. Montfort, P. Marquet, and C. Depeursinge, "Automatic procedure for aberration compensation in digital holographic microscopy and applications to specimen shape compensation," Appl. Opt. **45**, 851–863 (2006).
5. T. Colomb, J. Kühn, F. Charrière, C. Depeursinge, P. Marquet, and N. Aspert, "Total aberrations compensation in digital holographic microscopy with a reference conjugated hologram," Opt. Express **14**, 4300–4306 (2006).
6. T. Colomb, F. Montfort, J. Kühn, N. Aspert, E. Cuche, A. Marian, F. Charrière, S. Bourquin, P. Marquet, and C. Depeursinge, "Numerical parametric lens for shifting, magnification, and complete aberration compensation in digital holographic microscopy," J. Opt. Soc. Am. A **23** (2006) (to be published).
7. D. Malacara, ed., *Optical Shop Testing*, Wiley Series in Pure and Applied Optics (Wiley, 1992).
8. J. W. Goodman, *Introduction to Fourier Optics* (McGraw-Hill, 1968).
9. E. Cuche, P. Marquet, and C. Depeursinge, "Aperture apodization using cubic spline interpolation: application in digital holographic microscopy," Opt. Commun. **182**, 59–69 (2000).
10. E. Cuche, P. Marquet, and C. Depeursinge, "Spatial filtering for zero-order and twin-image elimination in digital off-axis holography," Appl. Opt. **39**, 4070–4075 (2000).
11. J. W. Goodman and R. W. Lawrence, "Digital image formation from electronically detected holograms," Appl. Phys. Lett. **11**, 77–79 (1967).
12. T. H. Demetrakopoulos and R. Mittra, "Digital and optical reconstruction of images from suboptical diffraction patterns," Appl. Opt. **13**, 665–670 (1974).